▌**Donor–Acceptor Systems** │*Hot Paper*│

Highly Segregated Lamello-Columnar Mesophase Organizations and Fast Charge Carrier Mobility in New Discotic Donor–Acceptor Triads

Ke-Qing Zhao,*[a] Ling-Ling An,[a] Xiao-Bo Zhang,[a] Wen-Hao Yu,[a] Ping Hu,[a] Bi-Qin Wang,[a] Jing Xu,[b] Qing-Dao Zeng,*[b] Hirosato Monobe,[c] Yo Shimizu,*[c] Benoît Heinrich,[d] and Bertrand Donnio*[d, e]

Abstract: Four new donor–acceptor triads (D–A–D) based on discotic and arylene mesogens have been synthesized by using Sonogashira coupling and cyclization reactions. This family of triads consists of two side-on pending triphenylene mesogens, acting as the electron-donating groups (D), laterally connected through short lipophilic spacers to a central perylenediimide (PI), benzo[*ghi*]perylenediimide (BI), or coronenediimide (CI) molecular unit, respectively, playing the role of the electron acceptor (A). All D–A–D triads self-organize to form a lamello-columnar oblique mesophase, with a highly segregated donor–acceptor (D–A) heterojunction organization, consequent to efficient molecular self-sorting. The structure consists in the regular alternation of two disrupted rows of triphenylene columns and a continuous row of diimine species. High-resolution STM images demonstrate that PI-TP2 forms stable 2D self-assembly nanostructures with some various degrees of regularity, whereas the other triads do not self-organize into ordered architectures. The electron-transport mobility of CI-TP2, measured by time-of-flight at 200 °C in the mesophase, is one order of magnitude higher than the hole mobility. By means of this specific molecular designing idea, we realized and demonstrated for the first time the so-called p–n heterojunction at the molecular level in which the electron-rich triphenylene columns act as the hole transient pathways, and the coronenediimide stacks form the electron-transport channels.

[a] Prof. Dr. K.-Q. Zhao, L.-L. An, X.-B. Zhang, W.-H. Yu, Prof. P. Hu, Prof. B.-Q. Wang
College of Chemistry and Materials Science, Sichuan Normal University
Jing-An Road 5, Chengdu 610066 (China)
E-mail: kqzhao@sicnu.edu.cn

[b] J. Xu, Dr. Q.-D. Zeng
CAS Key Laboratory of Standardization and Measurement for Nanotechnology, National Center for Nanoscience and Technology (NCNST)
11 Zhongguancun Beiyitiao, Beijing 100190 (China)
E-mail: zengqd@nanoctr.cn

[c] Dr. H. Monobe, Dr. Y. Shimizu
Inorganic Functional Materials Research Institute
National Institute of Advanced Industrial Science and Technology (AIST)
Ikeda, Osaka 563-8577 (Japan)
E-mail: yo-shimizu@aist.go.jp

[d] Dr. B. Heinrich, Dr. B. Donnio
Institut de Physique et Chimie des Matériaux de Strasbourg (IPCMS)
CNRS-Université de Strasbourg (UMR 7504), 23 rue du Loess, BP 43
67034 Strasbourg Cedex 2 (France)
E-mail: bertrand.donnio@ipcms.unistra.fr

[e] Dr. B. Donnio
Complex Assemblies of Soft Matter Laboratory (COMPASS), CNRS-Solvay University of Pennsylvania (UMI 3254), CRTB
350 George Patterson Boulevard, Bristol, PA 19007 (USA)

Supporting information for this article is available on the WWW under http://dx.doi.org/10.1002/chem.201500889 (including the detailed synthetic procedures of all compounds, ¹H and ¹³C NMR spectra, HRMS, and IR spectra, TGA and DSC traces, SAXS profiles, photocurrent vs. time curves, POM and STM images in color, UV and PL in solution and solid state in color).

Introduction

Since their discovery in 1977,[1] discotic liquid crystals (DLCs) have been attracting considerable interests for their distinctive features such as self-organization into liquid-crystalline columnar mesophases, self-healing of organizational defects, one-dimensional charge migration, and a wide range of potential applications in low-cost solution-processed organic thin-film electronic devices.[2–18] DLCs are molecules consisting usually of a large π-conjugated polycyclic aromatic core peripherally equipped by six-to-eight diverging alkyl chains. Such a specific molecular shape incites the molecules to stack into columns, which further self-organize into various two-dimensional lattices. Within these columns, the overlapped π-orbitals between close, adjacent molecules form the inner conducting pathway and allow one-dimensional charge transport, whereas the surrounding flexible alkyl chains play the role of soft insulators between adjacent columns. Among the large diversity of DLCs that have been synthesized in recent years, triphenylene- and perylenediimide-containing liquid crystals are particularly attractive materials for such prospects.[2, 3]

DLCs based on triphenylene (TP) derivatives have now been extensively studied: Their synthetic chemistry is versatile and well-developed,[2, 10] pure compounds are available by column chromatography and recrystallization, large area homeotropic alignments are preferred, and as far as their semi-conductive

performances are concerned, the hole mobility (μ_{h+}) of triphenylene discogens has been measured in the range of 10^{-4} to 10^{-1} cm^{2}V^{-1}s^{-1} depending on the degree of order of the columnar mesophases.[19–22]

As for perylenediimide (PI) derivatives, they are important chromophores and fluorophores with prominent thermal and photochemical stability, and have been studied as n-type semiconductors.[23–27] The liquid crystalline properties of PI derivatives, their semi-conducting properties, as well as their performance in electronic devices have been largely investigated.[28–37] PI-based mesogens show rich self-organization properties, are soluble in organic solvents, and are attractive candidate electron-acceptor materials for the replacement of fullerene derivatives in organic photovoltaic solar cells.[33,34] Furthermore, PI is a versatile synthetic building block and the discogens based on this structural motif, such as π-conjugation extended coronenediimide (CI) and coronenemonoimide, have been synthesized and found to exhibit ordered self-organized architectures and fast local charge carrier mobility.[38–42]

The molecular engineering of covalently linking electron donor (D) and electron acceptor (A) in D–A molecular systems is relevant for realizing the so-called "molecular heterojunction", which appears to be the ideal device configuration for the photoinduced energy and charge transfer and for the charge collection and transport, in artificial photosynthesis and organic photovoltaic solar cells.[43–59] Supramolecular organizations of self-assembled D–A systems with total segregation at the molecular level, fostered by self-sorting, and the formation of two distinct and active conductive pathways are indeed highly desirable for performance improvements of light-emitting diodes and photovoltaic devices, but they are also challenging to realize. To achieve this goal, the effect of molecular symmetry and rigid core incompatibility,[49,50] side-chain incompatibility and amphiphilic side-chains,[51–54] as well as molecular chirality[57] on the assembly behaviors have been investigated. Although, higher charge carrier mobilities have been essentially observed in such segregated stacking systems, most of them have been realized in solutions only, therefore without the implication of the liquid crystalline ordering. It is thus essential to design new covalently linked D–A oligomeric systems based on discotic mesogens that should lead to highly segregated assemblies in the liquid crystalline state.

Until now, only two examples of triphenylene-perylene donor–acceptor mesomorphic oligomers[58,59] have been reported, but segregation between triphenylene and perylene units was not realized in the self-organized structures, likely consequent to the long spacer separating both the active moieties. In the light of these promising results, we undertook to further vary the molecular design and to increase the size of the conjugated segments, in the hope to force the formation of segregated A and D zones by self-sorting and to preserve a mesomorphic structure with positional long-range order. In this case we designed a D–A–D triad architecture that combines triphenylene as the classical p-type moiety (D), perylenediimide or coronenediimide as standard or large-size n-type pseudo-discotic cores (A) and lateral attachment through short aliphatic spacers (Figure 1). Short spacers between D and ar-
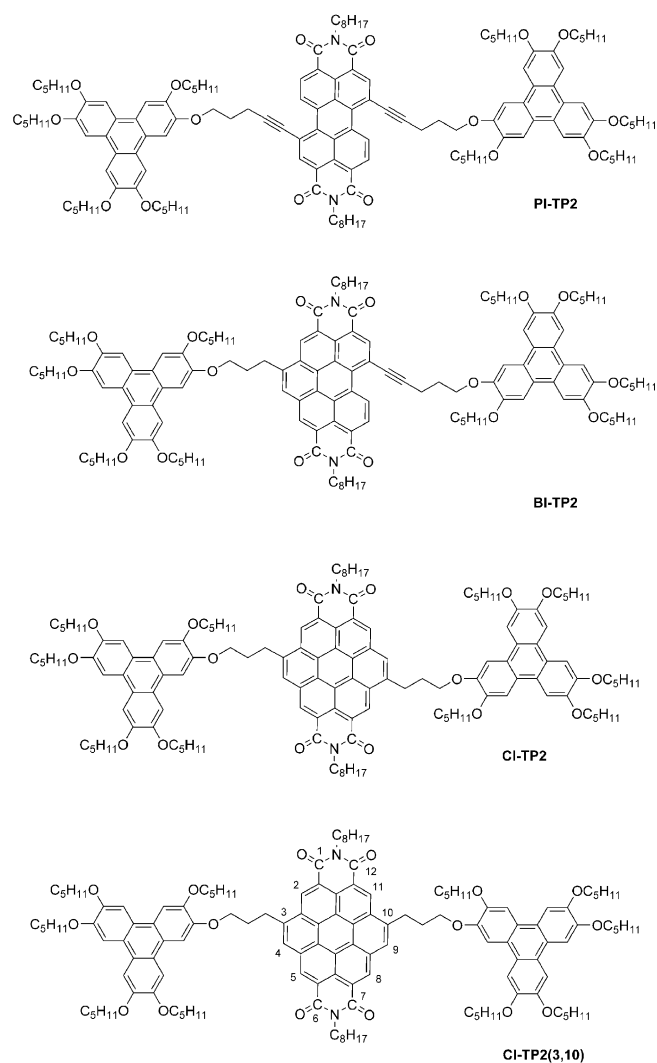
Figure 1. Molecular structures of the donor–acceptor (D–A) discotic-based triads, PI-TP2, BI-TP2, CI-TP2 and regioisomer CI-TP2(3,10).

omatic cores guarantee the electronic active discogens possessing partial freedoms of intracolumnar rotation and fluctuation, which are key parameters for determining charge carrier mobility along the discotic columns,[60] however avoid their mutual overlapping.

In the successive following sections, we report on 1) the molecular design and synthesis of four D–A–D discotic-based triads; 2) the characterization of the resulting hierarchical self-organizations in the bulk mesophase and demonstrate that donors and acceptors self-sort and fully segregate into separate columns with a regular alternation of rows of triphenylene and diimine columns (SAXS); 3) the stable 2D self-assembly nanostructures of PI-TP2 on HOPG/liquid interfaces (STM) with some various degrees of regularity, reminiscent of the mesophase ordering, and finally, 4) the electronic charge transport properties, and in particularly, on the remarkably long-range ($\approx$15 μm) electrons and holes mobilities, unambiguously measured by time-of-flight (TOF), which support the existence of two types of separated positive and negative charge carrier pathways.

Results and Discussion

Molecular engineering, synthesis, regioisomer separation and characterization

Subtle relationships exist between the molecular structures of perylene-triphenylene oligomers and their ability to exhibit mesomorphism. Cammidge et al.[58] synthesized triads consisting of two TP discogens terminally linked to both extremities of a PI central core with flexible aliphatic spacers: The triads with shorter soft spacers, for example, $(CH_2)_2$, $(CH_2)_4$, and $(CH_2)_6$, did not show mesomorphism; however, one triad with a longer spacer $(CH_2)_{10}$ for decoupling of the rigid cores displayed columnar mesophases, but with undifferentiated stacking of TP and PI cores. Gupta et al.[59] reported a perylenetetra-carboxylate tetraester of TP, with the side-discogens being decoupled from the core by long spacers, $(CH_2)_{12}$, which showed a hexagonal columnar mesophase, again with a mixed TP and perylene cores stacking. These results demonstrate that D–A segregated organization for PI/TP LC-based oligomers still remains a challenge. In the molecular design proposed in this study, the TP groups are selectively connected by short spacers at two of the bay positions of a central perylenediimide derivative (Figure 1) to yield a more constrained system than those described above. Self-sorting, originating from mismatched intermolecular interactions and molecular shapes, is thus expected to foster supramolecular arrangements with the differentiation between the two molecular active species at play, and their eventual stacking into distinct columns.

To ensure solubility and eventually mesomorphism with such D–A-like triad architectures (Figure 1), we first designed the functional unsymmetrical TP discogen possessing short side chains (pentyloxy) and a terminal alkyne (pent-4-yn-oxy), and a PI central unit with two axial N-octyl chains. The triad was then synthesized by the Sonogashira coupling reaction between functional TP and PI, beforehand functionalized at the two bay positions with bromine (2Br-PDI, Scheme 1).

Perylenetetracarboxylic dianhydride was first brominated with bromine and then iminated with n-octylamine according to literature methods.[38,39] The other intermediate alkynyl-triphenylene (alkynyl-TP), was synthesized by the etherification of the monohydroxytriphenylene as previously reported.[61,62] The Sonogashira coupling reaction catalyzed by using [Pd(PPh3)4] between 1,7-dibromo-PI (2Br-PDI) and alkynyl-TP was carried out in Et3N-toluene to successfully produce the triad PI-TP2 in yield of 78%, along a small amount of the half-annulated product BI-TP2 (5.9%) (Scheme 1). Furthermore, the Sonogashira coupling catalyzed by [PdCl2(PPh3)2]/CuI ran in the Et3N/THF solvent mixture produced PI-TP2 in 63% yield, whereas when performed in Et3N/pyridine directly, it produced the half-cyclized BI-TP2 (41% in one-pot). The use of the strong organic base 1,8-diazabicyclo[5.4.0]undec-7-ene (DBU) promoted the cyclization of PI-TP2 to give BI-TP2 and CI-TP2 isolated in 42 and 31% yield, respectively. Further, BI-TP2 in toluene with 10 mol% DBU was transformed into CI-TP2 in a yield of 69%. The triads were purified by column chromatography (silica gel, eluting with CH_2Cl_2) and recrystallization from
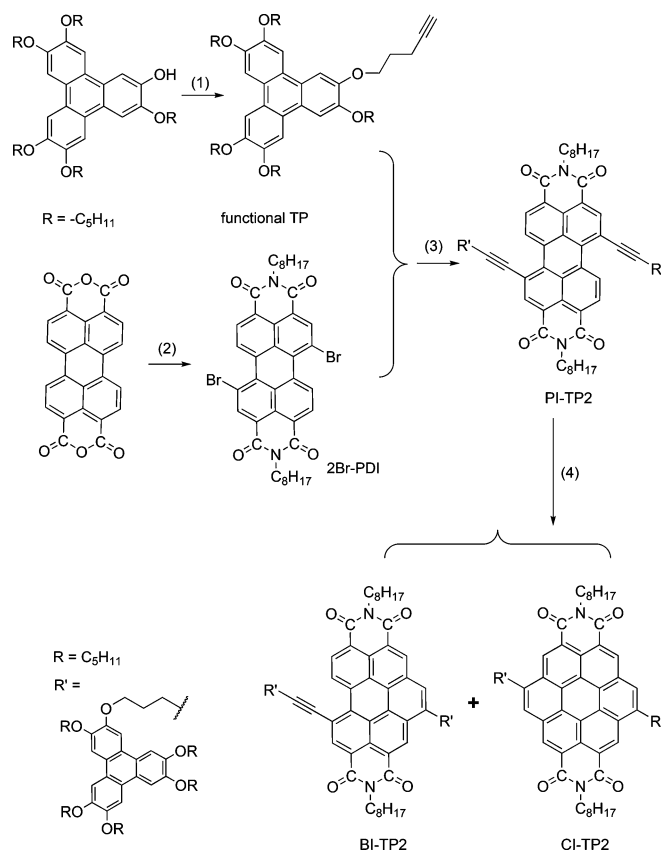
Scheme 1. Synthesis of donor–acceptor–donor (D–A–D) discotic-based triads, PI-TP2, BI-TP2, and CI-TP2 isomers. Reaction conditions [yields]: (1) 5-chloropent-1-yne, K_2CO_3, DMF, 60°C, 24 h [64%]; (2) (a) Br_2, 98% H_2SO_4, 80°C, 20 h [58%]; (b) CH_3CH_2COOH, $C_8H_{17}NH_2$, 160°C, 24 h [60%]; (3) [Pd(PPh3)4], Et3N/PhMe, argon atmosphere, 90°C, 22 h [78%]; or [Pd(PPh3)2Cl2]/CuI, Et3N/THF, 80°C, 24 h [63%]. (4) 1,8-diazabicyclo[5.4.0]undec-7-ene (DBU), PhMe, 90°C, 24 h, argon atmosphere, CI-TP2 [31%] and BI-TP2 [42%].

organic solvents (synthetic details and characterizations are given in the Supporting Information).

The synthesis of these triads by Sonogashira coupling and organic base-promoted cyclization reactions have been repeated several times and shown remarkable reproducibility and stable yields. PI-TP2 has been synthesized in yield of 78% catalyzed by [Pd(PPh3)4], higher than the catalysis of [Pd(PPh3)2Cl2]/CuI (63%). The strength of the organic base has shown a strong impact on the cyclization reaction: With Et3N as the base, the main product is PI-TP2; with Et3N/pyridine as the base and solvent, BI-TP2 is produced in one pot; finally, 10 mol% DBU efficiently catalyzed the cyclization of PI-TP2 and BI-TP2 to CI-TP2. The results have demonstrated that the stronger the base, the more efficient the cyclization reaction.

Wurthner et al.[63] reported that the bromination of perylene-tetracarboxylic acid dianhydride (PTCDA) resulted in mainly 1,7- and 1,6-dibrominated products, with a small amount of mono- and tribrominated byproducts. We used this method to prepare the dibromo-PTCDA precursor. However, due to their low solubility in organic solvents, the various brominated compounds could not be separated, and we directly proceeded to the imidization reaction with n-octylamine. At this stage the

products were soluble, and the mono- and tri-brominated PIs were easily discarded as byproducts, whereas the di-brominated PIs were collected as a mixture of 1,7- and 1,6-dibromo regioisomers, which could not be separated by column chromatography. 600 MHz ^{1}H NMR spectroscopy permitted to estimate the ratio between both the 1,7- and 1,6-regioisomer as 100:15.

The Sonogashira coupling between 2 Br-PI and alkynyl-TP produced PI-TP2 composed mainly of the 1,7-substituted isomer with a residual amount of the 1,6-isomer, which could not be separated by column chromatography (the ratio of isomers was found almost unchanged, 100:12, as differentiated by NMR spectroscopy). The half-annulated product, BI-TP2, should consist of the same ratio of regioisomer, even though the high-resolution NMR spectroscopy did not permit to discriminate both the isomers. Unexpectedly, the annulated product CI-TP2 and its regioisomer, CI-TP2(3,10), were successfully separated by column chromatography (silica gel, eluting with CH$_2$Cl$_2$), yielding the regioisomerically pure forms, that is, 3,9- and 3,10-disubstituted coronenediimide, in the ratio of about 10:1. The less polar regioisomer in smaller amounts was assigned to the CI-TP2(3,10), the main isomer with 3,9-disubstitution as CI-TP2. The four triads have been fully characterized by HRMS, IR (the Supporting Information), and UV/Vis absorption and fluorescence emission spectroscopies.

UV/Vis absorptions and fluorescent emissions

UV/Vis was recorded in solution for all triads. They displayed well-separated absorption bands of the TP and arylene diimide chromophores, respectively (Figure 2). All four triads have a strong absorption peak at 277 nm, originating from the triphenylene part; the other absorption bands between 300–600 nm are characteristic bands of aryldiimides (Table 1). The absence of characteristic charge-transfer bands at longer wavelength demonstrates that the charge transfer complex does not form between the D and A moieties of the molecules at ambient condition. The absorption bands showed obvious blueshift from PI to BI, then to CI as the chromophores frontier molecular orbital energy gap increases. The broad UV/Vis absorption bands of triads between 400–600 nm imply that the blend of these triads would have good sunlight harvesting and could be applied as optoelectronic materials.

Steady-state fluorescence emission spectra of the triads were measured for investigating the D–A intramolecular energy and electronic transfer as TP and diimide part excited separately (Figure 2, Table 1). PI-TP2 showed 65% emission quenching of TP and the complete quenching of PI. As the fluorescence spectrum of TP has no overlap with the absorption spectrum of PI, intramolecular Forster energy transfer do not exist in this triad, and therefore the quenching is essentially caused by Dexter electron transfer between TP and PI, independently of the excitation wavelength (277 or 547 nm). However, BI-TP2 and both CI-TP2 isomers showed complete fluorescence quenching of the TP part and strong emission of the aryldiimide part, independently of the species excited, for example, the donor (TP) or the acceptor (BI or CI). As the fluorescence emission spectrum of TP has overlap with the ab-
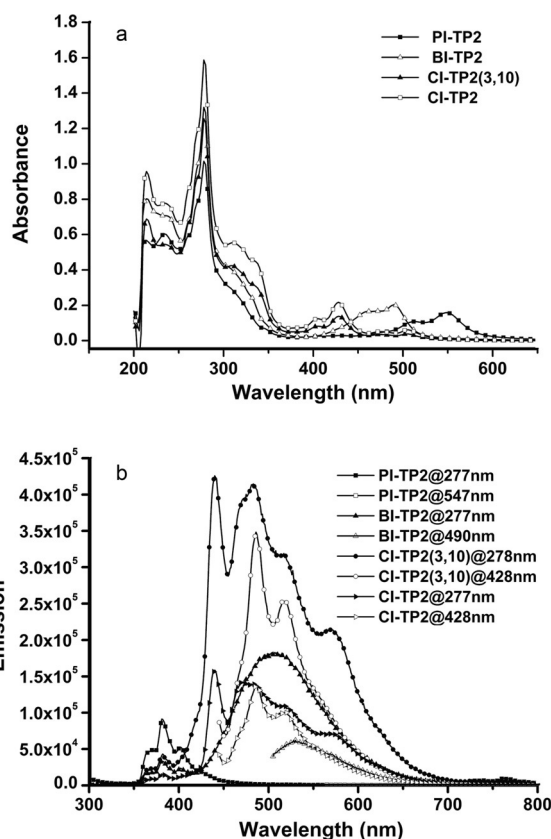
Figure 2. a) UV/Vis absorption spectra of the four triads. b) Fluorescent emission spectra of the triads with excitation of TP and the diimide, respectively. Concentration of samples: 5.0×10^{-6} M in THF.

Table 1. Optical properties of UV/Vis absorption and fluorescent emission of the triads.[a]

	λ_{abs} [nm]	ε [L mol^{-1} cm^{-1}]	λ_{em} [nm]
PI-TP2[b]	278	2.1×10^{5}	381
	548	3.2×10^{4}	_[b]
BI-TP2	278	2.6×10^{5}	507
	490	4.1×10^{4}	530
CI-TP2(3,10)	278	2.5×10^{5}	485
	428	2.8×10^{4}	486
CI-TP2	278	3.2×10^{5}	485
	428	4.3×10^{4}	486

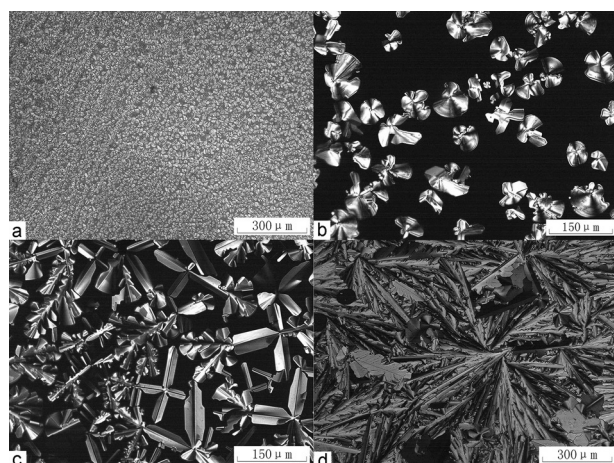[a] In THF: 5×10^{-6} mol L^{-1}. [b] PI-TP2 excited at 547 nm did not display emission.

sorption spectra of BI and CI, intramolecular Forster energy transfer occurs within the triads (BI-TP2 and both CI-TP2 isomers).

PI is a well-known n-type semiconductor and shows a stronger electron-accepting ability than that of the BI and CI core moieties, which may explain the photophysical property differences of these triads: Intramolecular electron transfer in PI-TP2 and intramolecular energy transfer for the other three triads. It is also noted that CI-TP2(3,10) showed weaker absorption but stronger emission than the regioisomer of CI-TP2, so the former is a better fluorophore. Both UV and photoluminescence have also been measured on solid films made of these

materials. UV absorption spectra display similar features, slightly broadened, than those recorded in solution, and no fluorescent emission was observed upon excitation of the arylenediimide core units (Figure S13 in the Supporting Information).
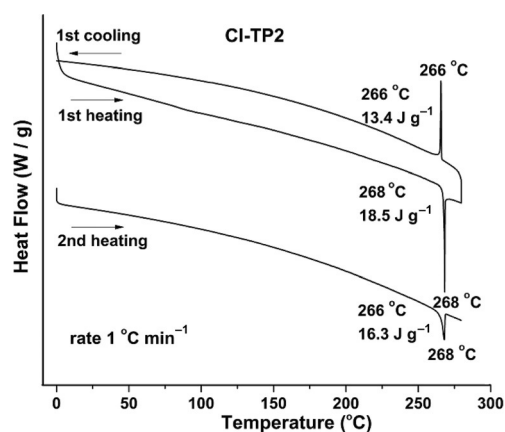
TGA, DSC, and POM investigations

Prior to the investigation of the LC behavior of the triads, their thermal stability was checked by thermal gravimetric analysis (TGA, the Supporting Information). The TGA measurements revealed the high thermal stability of the triads with decomposition temperatures (defined as the onset temperature at 5% weight loss) being above 380 °C (the Supporting Information, Figure S7). The mesomorphic properties were then first evaluated by polarized optical microscopy (POM) and differential scanning calorimetry (DSC). Large homogeneous, birefringent domains typical of columnar mesophases were observed by POM for samples of BI-TP2, CI-TP2, and CI-TP(3,10) on slow cooling from the isotropic liquid: BI-TP2 showed fan-like textures, CI-TP2 exhibited mosaic texture with dendritic domains, whereas CI-TP(3,10) gave mainly dendritic and leaf-like textures (Figure 3). However, PI-TP2 in contrast showed non-characteris-

Figure 4. DSC curves of the triad CI-TP2, selected as a representative example. The curves of first heating and cooling, and the second heating runs were measured under nitrogen at a rate of 1 °C min^{-1}. Peak temperatures, onset temperatures, and enthalpy changes are directly labelled on the traces, or close to the transition peaks.

Figure 3. POM textures of the LamCol$_{obl}$ phase (see main text) of the triads a) PI-TP2, b) BI-TP2, c) CI-TP2, and d) CI-TP2(3,10) observed on cooling from the isotropic liquid.

cooling curves, whereas PI-TP2 did not show obvious reversibility between endo- or exo-thermal cycles, confirming the POM observations and the possible thermal oligomerization. The DSC phase transition data are summarized in Table 2.

Mesophase characterization by SAXS

The trimeric triphenylene-containing compounds exhibit the same LC mesophase, namely, a lamello-columnar phase with an oblique 2D symmetry, thereafter designed as LamCol$_{obl}$, as clearly identified by SAXS. The diffractograms recorded in the mesophase at various temperatures (Figure 5 a–c and the Supporting Information, Figure S10), all invariably exhibit a similar pattern: A set of six (for CI-TP2) to eleven (for BI-TP2) sharp reflections in the small-angle range ($2° < 2\theta < 15°$), a strong and broad wide-angle signal with a maximum at about 4.5–4.6 Å associated with the scattering arising from lateral distances between molten chains (h_{ch}), and another less intense, semi-sharp scattering signal resulting from the short-range π–π stacking interactions, mutually associated with the various central arylene cores (PI, BI, CI) and TP moieties (undifferentiated maxima,

tic, small birefringent domains in the fast cooling from isotropic liquid due to plausible thermal oligomerization occurring at such a high temperature combined with intense light exposure (the isotropic temperature is determined at about 210 °C). The thermally treated sample of PI-TP2 was characterized by using ^{1}H NMR spectroscopy, showing polymer-like broad peaks, and the high-resolution mass spectrum revealed the formation of at least dimers (higher oligomers cannot be measured as they out of the upper limitation of the mass instrument; see the Supporting Information, Figure S9).[64] The DSC curves of the other three triads (Figure 4 and the Supporting Information, Figure S8) showed reversible heating and

Table 2. Thermal and thermodynamic properties of triads by POM and DSC (10 °C min^{-1}).[a]

Triad	Second heating Transition temperature [°C, peak maximum] and enthalpy change (ΔH [J g^{-1}])	First cooling Transition temperature [°C] and enthalpy change (ΔH [J g^{-1}])
PI-TP2[b]	LamCol$_{obl}$ 210 (9)	–
BI-TP2	LamCol$_{obl}$ 269 (17) I	I 245 (7) LamCol$_{obl}$
CI-TP2	LamCol$_{obl}$ 268 (16) I	I 266 (13) LamCol$_{obl}$
CI-TP2(3,10)	LamCol$_{obl}$ 263 (16) I	I 259 (15) LamCol$_{obl}$

[a] LamCol$_{obl}$: Lamello-Columnar mesophase with oblique two-dimensional symmetry (see text); I: Isotropic liquid. [b] For PI-TP2, thermal oligomerization occurring at 210 °C, no obvious phase transition was observed on cooling from DSC curve (see main text).
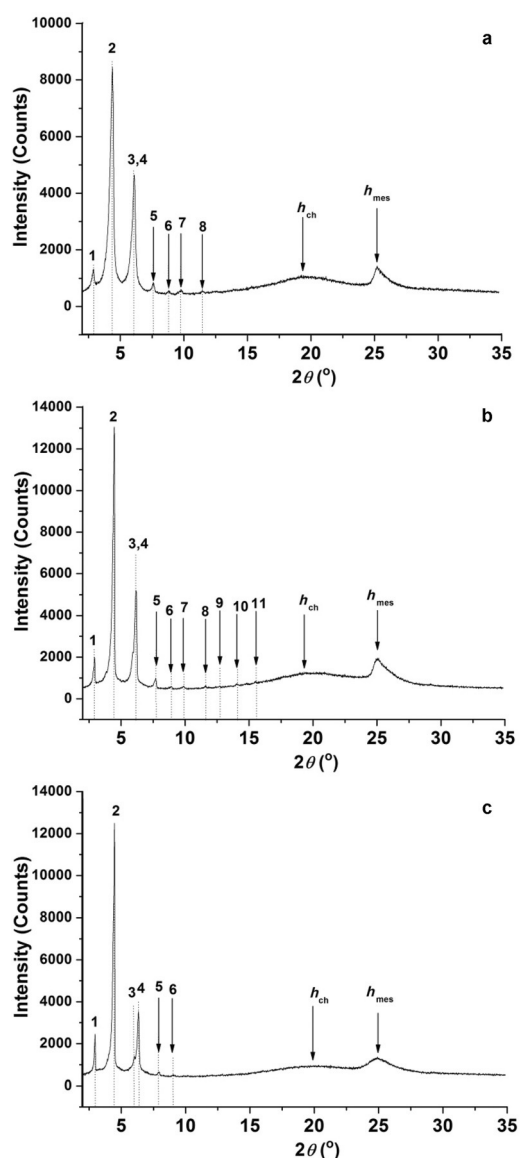
Figure 5. Representative SAXS patterns of triads a) PI-TP2, b) BI-TP2, and c) CI-TP2 at room temperature.

$h_{mes} = h_{core} + h_{TP}$ at 3.53, 3.55, and at 3.57 Å for the PI-TP2, BI-TP2, and CI-TP2 diimine derivatives, respectively, Figure 5 a–c).

The large number of small-angle reflections unambiguously permitted the assignment of 2D oblique lattices, by using home-developed indexation software. Lattice parameters turned out to be very similar for the three triads (see Table 3, $a = 68.6$–69.8 Å, $b = 14.5$–14.8 Å, and $\gamma = 119$–122°), with areas compatible with the accommodation of one entire triad, that is, of a single molecular stack generating three differentiated columns (i.e., two TP- and one arylene-based columns). The presence of several (h0) reflections suggests a layering within this supramolecular organization. In particularly, the intense reflection (30) (reflection 2 in Figure 5 a–c) implies a tripling of the unit cell with the alternation of three rows of high-electronic density separated by the low-electronic density aliphatic continuum. A peculiar feature of this structure is that the oblique symmetry is observed for columns with quasi non-tilted

stacking of the diimine cores and triphenylene (as the molecular thickness h_{mol}, ratio of molecular volumes V_{mol} and of lattice areas A, are similar to stacking distances $h_{mes} = h_{core} + h_{TP}$, see Table 3), and likely arises from the staggered disposition of the diimine derivatives in rows, rejecting the laterally attached triphenylene mesogens on each side.

Diimide cores and triphenylene units, independently, stack into columns to form regions of high electronic density, separated from each other by the aliphatic chains that form a continuum of low electronic density. This designs a smaller oblique sub-lattice with only one single column and fundamental periodicities corresponding to the reflections (3−1), (60) and (31) of the large lattice (reflections 3, 6, 7, Figure 5 a–c). However, diimine and triphenylene are expected indeed to be segregated at the molecular level and generate two types of columns, whose differentiation in the structure is proven by the presence of the reflections (11), (1−1), and (20) of the large lattice (reflections 1, 4, 5, Figure 5 a–c, Table 2).

The relative intensity exaltation of the (20) reflection, with respect to reflections (11) and (1−1) then would indicate that rows formed by the diimine-columns lie parallel to this reflection. Further, the strong enhancement of the intensity of the (30) reflection implies that these diimine-forming rows are not disrupted but rather continuous (the central cores are mutually in close contact through the edges, which is possible because they are not truly discotic in shape but rather lath-like), and, because of the specific molecular topology of the triads (side-on attachment of TP groups), two intermediate strata containing triphenylenes are generated between successive rows of diimines.

The high intensity of the reflections characterizes the long-range correlated structure of the mesophases. It should be mentioned that two intense small scattering maxima are steadily visible in the patterns above the isotropization temperature, at about the same positions as the reflections 2 and 3 of the LamCol$_{obl}$ phase, with correlation lengths around 100–150 Å (the Supporting Information, Figure S10). The nanosegregation between TP, chains and PI/BI/CI, reminiscent of the supramolecular organization, is consequently preserved despite the disappearance of the long-range positional and orientational orders, and highlights the strong incompatibility of both mesogens. A related feature in the mesophase consists of the asymmetric shape of the h_{mes} scattering, with the usual slight broadening of the wide-angle wing and the unconventional sharpness of the small-angle wing (Figure 5). The former simply reflects the fluid character of the mesophase and sliding from the optimal stacking position. The differentiated column row alternation nevertheless maintains the mesogens of each type in close contact and extends the stacks to correlation lengths in the order of 300 Å.

Based on this structural analysis, one can propose the following model for the supramolecular organization of the triads that renders a good account of the observed reflections intensities distribution. It would consist of the alternation of a disrupted double-row of triphenylene mesogens flanked by a single continuous row of diimine species, as shown in Figure 6; the tilt angle may be simply due to the presence of

Table 3. Indexation of the mesophase of the triads.[a]

No.	$2\theta_{exp}$	d_{exp}	I [%]	hk	$2\theta_{cal}$	d_{cal}	Mesophase parameters
				Triad PI-TP2			
1	2.88	30.65	7.5	20	2.918	30.25	LamCol$_{obl}$
2	4.38	20.16	100	30	4.377	20.17	$a = 69.3(6)$ Å
3	6.119	14.43	52	3–1	6.065	14.56	$b = 14.7(75)$ Å
4	–	–	–	1–1	6.269	14.09	$\gamma = 119.2(6)°$
5	7.60	11.62	4.31	11	7.673	11.51	$A = 894$ Å²
6	8.807	10.03	1.6	60	8.761	10.08	(h_{mes}; $N=1$, $Z=3$)
7	9.808	9.01	2.1	31	9.776	9.04	$V_{mol} = 3122 \pm 100$ Å³
8	11.45	7.72	1.4	9–1	11.481	7.70	$h_{mol} = V_{mol}/A = 3.49$ Å
	19.5	4.55	–	h_{ch}	–	–	
	25.22	3.53	8.4	h_{mes}	–	–	
				Triad BI-TP2			
1	2.929	30.14	10	20	2.949	29.94	LamCol$_{obl}$
2	4.46	19.79	100	30	4.423	19.96	$a = 68.6$ (6) Å
3	6.16	14.34	37	3–1	6.141	14.38	$b = 14.5(86)$ Å
4	–	–		1–1	6.353	13.90	$\gamma = 119.3°$
5	7.719	11.44	3.7	11	7.774	11.36	$A = 873$ Å²
6	8.911	9.92	0.9	60	8.854	9.98	(h_{mes}; $N=1$, $Z=3$)
7	9.92	8.91	1.0	31	9.899	8.93	$V_{mol} = 3101 \pm 100$ Å³
8	11.56	7.68	0.7	9–1	11.598	7.62	$h_{mol} = V_{mol}/A = 3.55$ Å
9	12.71	6.96	0.5	2–2	12.725	6.95	
10	14.05	6.3	0.8	02	13.913	6.36	
11	15.48	5.72	0.7	22	15.584	5.68	
	19.5	4.55	–	h_{ch}	–	–	
	25.03	3.55	7.5	h_{mes}	–	–	
				Triad CI-TP2			
1	2.959	29.83	17	20	2.988	29.55	LamCol$_{obl}$
2	4.452	19.83	100	30	4.482	19.70	$a = 69.8$ Å
3	5.981	14.76	6.5	3–1	5.977	14.77	$b = 14.8(94)$ Å
4	6.34	13.93	29	1–1	6.336	13.94	$\gamma = 122.1(5)°$
5	7.902	11.18	1.6	11	7.903	11.18	$A = 880$ Å²
6	9.033	9.78	0.9	60	8.971	9.85	(h_{mes}; $N=1$, $Z=3$)
	19.5	4.55	–	h_{ch}	–	–	$V_{mol} = 3080 \pm 100$ Å³
	24.92	3.57	5.0	h_{mes}	–	–	$h_{mol} = V_{mol}/A = 3.50$ Å

[a] No. represents the reflection numbers (see Figure 5); $2\theta_{exp}$, $2\theta_{cal}$, d_{exp} and d_{cal} are the experimentally measured and calculated diffraction angles [°] and distances [Å]; $d_{meas.} = \lambda/(2\sin\theta_{exp})$, and $2\theta_{cal} = 2\arcsin[\lambda/(2d_{cal})]$; I corresponds to the relative intensity of the reflections (given for the sharp reflections); hk are the Miller indices of the reflections; h_{ch} and h_{mes} ($=h_{TP}+h_{core}$) correspond to the maximum of the diffuse scattering due to lateral distances between molten aliphatic tails (h_{ch}) and between stacked triphenylene and perylene mesogenic cores (h_{mes}), respectively; a, b, and γ are the lattice parameters of the oblique lattice; $d_{calc.}$, a, and b are deduced from the following mathematical expressions: $a = 2d_{20}/\sin\gamma$ and $b = (2/[1/(d_{11})^2 + 1/(d_{1-1})^2 - 1/2(d_{20})^2])^{1/2}/\sin\gamma$, and A the cell area from $A = a \cdot b \cdot \sin\gamma$; N and Z are the number of molecules and columns per lattice, respectively; V_{mol} is the molecular volume, and $h_{mol} = V_{mol}/A$ is the molecular thickness.

the two alkyl chains grafted at both extremities, which then are forced to shift laterally to reduce the spacing in the rows and accommodate with the spacing in the rows of TP. Note that the TP-forming rows are not necessarily in registry. Within this proposed supramolecular organization, it is anticipated that the segregation between both electron-donating and accepting species into distinct zones may lead to the formation of two differentiated active conduction pathways. A very similar mesophase structure has recently been proposed for structurally related systems, namely polythiophenes bearing TP side groups.[54]

## 2D self-organization of discotic triads studied by STM

The strengths of DLC-based semiconductors are their anisotropy, processability, self-assembling, and self-healing properties, which make them more suitable in fabricating electronic devices than small molecular crystals and even polymers. Although many favorable characteristics are reflected in the stacking direction constructed by π-conjugated systems, the behavior of these molecules on two-dimensional substrate should not be ignored. Since most electronic devices are supported by a conductive substrate, the interfacial region between substrate and organic semiconductor is of significant importance. Indeed, the orientation, conformation, packing patterns, and structural defects of interfacial layer may affect the rate of the carriers' mobility and even change the transportation pathways, which in turn will influence the performance of the corresponding molecular devices to a large extent.

Utilizing the variation of tunneling current, STM has the advantage of visualizing the position and distribution of molecules directly at the atomic level without damaging the samples.[65,66] It is therefore an ideally suited technique in detecting two-dimensional self-assembling processes at liquid–solid interfaces. Previously, STM has been employed in investigating aromatic molecules adsorption on a variety of substrates, including metals, semiconductors, and conductors. In particular, details of nanostructured self-assemblies and surface reactions involving phthalocyanine, porphyrin, pyrene, and their derivatives have been demonstrated by STM.[65,66]

Previous STM studies of PI and multimeric perylene derivatives showed that they could self-assemble with long-range ordering in some regions.[67,68] Similarly, STM studies have also been reported for coronene molecules. However, it was shown that they were often hard to detect when adsorbed solely on the highly oriented pyrolytic graphite (HOPG) substrate.[69] As a result, coronene derivatives were often introduced into a host molecular template to be immobilized as guest molecules. Previously, Zhang et al. have reported STM investigations of triphenylene-substituted pyrene derivatives.[70] The TP groups appeared like bright triangular points because of the high electron density of the four aromatic rings. In the present
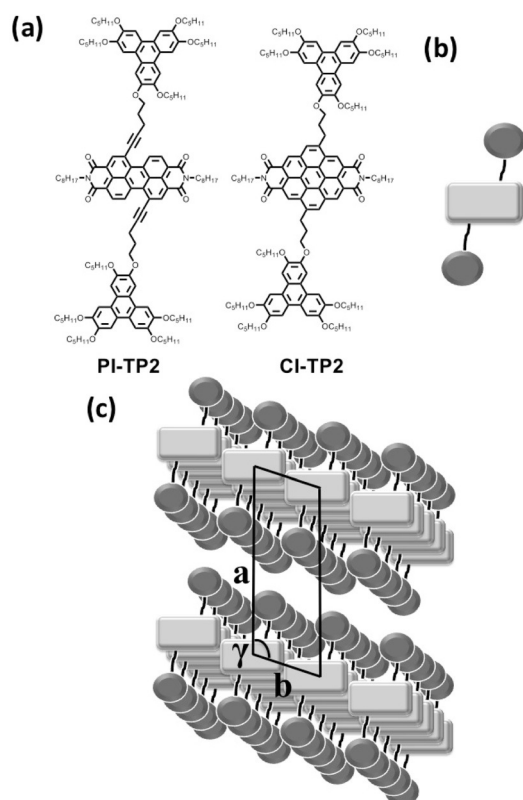
Figure 6. a) Molecular structures of triads PI-TP2 and CI-TP2; b) Molecular model; c) Proposed model for the LamCol$_{obl}$ mesophase (all triads): diimide cores generate a continuous row (light grey), alternating with rows of triphenylene cores stacked into columns (dark gray); the peripheral alkyl chains, omitted for clarity, fill all the available space; the black lines represent the 2D lattice, and a, b and γ, the oblique cell parameters.

work, the PI, BI, and CI aromatic cores are covalently linked to the TP discogens, from which attractive new features may arise in the interfacial region, besides the modified electronic property. 1-Phenyloctane was chosen as the solvent for STM imaging since it has a low vapor pressure and relatively weak interaction with HOPG substrate. Therefore, it will minimize the influence on target molecules adsorption.

Detailed arrangements of the 2D self-assembly of PI-TP2 on HOPG at the solid/liquid interface are presented in the high-resolution STM image of Figure 7 a. The candy-shaped PI-TP2 triad was constituted by three bright spots; a rectangular point in the center and two triangular-shaped spots on both sides. The central point could be ascribed to the PI part while the two side groups referred to TP groups. The PI groups appeared brighter than the TP groups because of their higher electron density. The long alkyl chains fill the dark zones of the image due to less contribution to the tunneling current. As far as we are aware, this is the first two-dimensional self-assembly reported with this pair of combinations.

Two types of packing patterns could be observed, marked as A and B, from scrutinized analysis of the high-resolution STM image (Figure 7 a). In domain A, three PI-TP2 molecules form a group, whereas in domain B, there are only two molecules. There is a slight dislocation between the two domains. A unit cell was imposed on each domain, respectively. In domai-
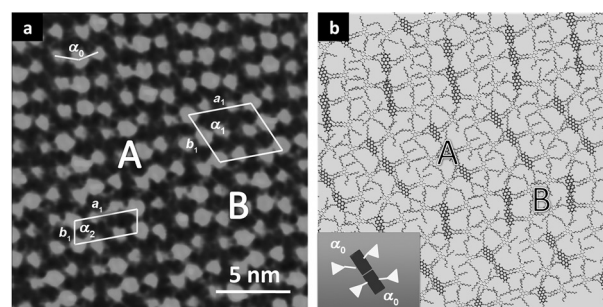
Figure 7. a) High-resolution STM image (20×20 nm) of PI-TP2. $I_{set}=349.1$ pA, $V_{bias}=599.1$ mV; b) Illustrated molecular model for a). In domain A, PI-TP2 molecules from three neighboring rows associate with close contacts between PI segments, while only two rows in domain B. Sub-image in b) shows a schematic illustration of the molecular packing in domain B. Lattices parameters: a_i, b_i, α_i.

n A, the measured parameters were $a_1=4.95$ nm, $b_1=3.96$ nm, and $\alpha_1=75.7°$. In domain B, the measured parameters were $a_2=4.95$ nm, $b_2=2.09$ nm, and $\alpha_2=82.8°$. An illustrative molecular model was proposed (Figure 7 b) to foster the understanding of packing arrangements (a schematic sub-image of domain B is inserted in the bottom left). The simplified model indicated that there might be a slight repulsion between the adjacent TP parts in one group of PI-TP2 molecules. The repulsive force caused an angle ($\alpha_0=162.8°$) within one PI-TP2 molecule.

Large-scale STM images of the PI-TP2 self-assembly provide direct insights of the structural details (Figure 8): Domains A, B, and C represent the three major regions within boundaries, highlighted with white and gray lines. The STM image demonstrated that the molecules exhibit some degrees of regularity in parallel rows (x direction, highlighted by arrow). However, in
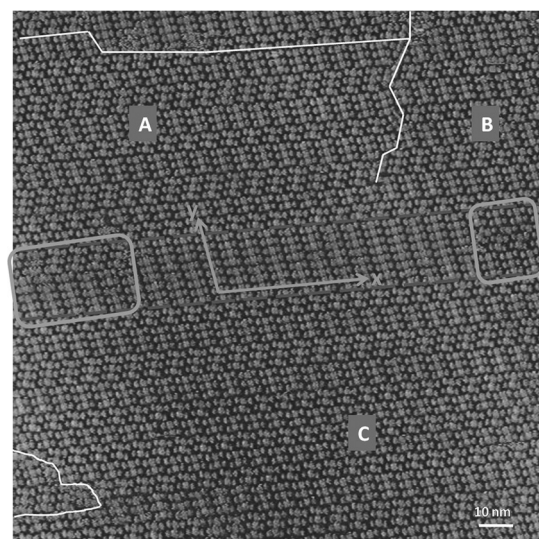
Figure 8. Large-scale STM image (120×120 nm) of PI-TP2. $I_{set}=299.1$ pA, $V_{bias}=599.1$ mV. A, B, and C represent the three major regions; white and grey lines mark their borders. The two dark-gray rectangular shapes show disorder parts in domain. The arrows represent the parallel direction (x) and the perpendicular packing axis direction (y).

the direction perpendicular to the rows (y direction, highlighted by arrow), various domains succeed and long-range order no longer exists. In each domain, several rows associate with close contacts between PI segments. Close contacts break and rows stagger at boundaries between domains.

Statistical results about the distribution of different packing patterns were obtained. The ratio of groups with two PI-TP2 molecules (43.80%) is similar to that with three PI-TP2 molecules (50.90%). These two packing patterns account for most of the regions. The STM Figure nevertheless displayed a region C with eight grouped rows of PI-TP2 molecules (borders marked with gray lines, Figure 8). However, the case was rare and may not be stable. There was also some kind of disordered zones at both ends (surrounded by the dark gray rectangles). It could be speculated that groups with less than four molecules were more stable under the current conditions. Since PI-TP2 is a LC material, this kind of disorder might enhance the liquid character, which is of significant importance in LC semiconductors.

According to the above discussion, PI-TP2 molecules could form stable 2D nanostructures on the HOPG substrate. High-resolution STM images could be obtained easily. However, we could not obtain satisfying STM data in terms of the assembling structures for the other three triad molecules. According to previous STM studies, stable adsorption of coronene derivatives like CI-TP2 was often hard to achieve, unless they were immobilized in host nano-networks.[69] The decrease or absence of ethynyl groups in BI-TP2 and CI-TP2, respectively, moreover increases the molecular flexibility and conformations, and allows molecules to easily twist or cluster. The shorter spacer between the rigid donor and acceptor of the molecules then makes STM imaging more difficult.

The 2D self-assembly structure of PI-TP2 is formed through van der Waals forces. STM figures revealed that molecules regularly align in parallel rows, but with irregular shifts between rows along the perpendicular packing axis. Meanwhile, the other three triads could not be observed by STM under these conditions because of the low affinity of these diimide cores with HOPG, the increasing molecular conformational disorder, and the shortening of the linkers between donor and acceptor groups. The molecular arrangement in the interfacial region is remarkably comparable to the model proposed for the columnar sub-lattice of the 3D bulk structure in the LamCol$_{obl}$ mesophase. The segregation pattern and the alternating rows structure is for instance the same, except that both in-plane packing directions are long-range correlated in the 3D structure and that lattice parameters are somewhat different. The domain A lattice thus shows almost the same angle (114 against 119°), a shrunken a-parameter (4.4 against 6.94 nm) and an expanded b-parameter (1.9 against 1.48 nm). These discrepancies reflect that PI-TP2 molecules involved in the solid/liquid interface arrangement interact with the graphite substrate, whereas interactions between stacked triads themselves determine the organization in the bulk. Furthermore, the triad molecules on the graphite surface form a sort of 2D crystal structure, whereas the 3D bulk organization is a fluid mesophase and involves dynamics with rotations and translations of

the molecules. The mesomorphic character also allows the spontaneous healing of self-organization defects and the development of long-range correlated segregated arrangements after thermal annealing and slow cooling of the samples.

Electron and hole mobility measured by using the time-of-flight technique

As we have just seen, the discotic-based triads display ordered LamCol$_{obl}$ mesophases, with differentiated columnar stacks in the bulk state, and PI-TP2 shows ordered self-assembly on HOPG/liquid interface. High charge carrier mobilities are therefore expected from the presence of the polycyclic π-conjugated aromatic cores and from their regular face-to-face stacking in the mesophases. TP discogens are indeed known as ambipolar mesomorphous semiconductors giving rise to one-dimensional columns, along which both electrons and holes are hopping,[21, 22] whereas PI and CI derivatives have shown electron-transporting properties suitable for n-type semiconductors.[36, 40]

Charge mobility is the most important parameter for organic semiconductors, as it determines the performance of the materials in electronic devices. There are mainly three techniques to measure the conductivity of LC semiconductors: Time-of-flight (TOF), pulse-radiolysis time-resolved microwave conductivity (PR-TRMC), and organic field-effect transistor (OFET). TOF and OFET techniques require that the molecules self-assemble according to different orientation patterns, and that the electronic charges hop along the column over a minimum distance of 10 μm. The PR-TRMC technique does not need well-ordered supramolecular organizations because it just measures the local charge transport over a few molecules only. Because it is difficult to control the alignment of discotic mesogens, huge differences occasionally occur between measured mobilities, making comparisons often difficult. One of the advantages of the TOF method is that the hole and the electron mobility can be obtained directly and independently and that both can be faced accurately.

Considering the similarity of the chemical structures of the three triads and their supramolecular organization, the charge mobility of one representative triad has been investigated. In particular, the most thermally stable compound, CI-TP2, was selected for the measurements, to gain reliable results; the other two compounds showing, as described above, some structural modifications upon heating. The charge carrier mobility of CI-TP2 sample in LC cell has been measured by the TOF technique in standard conditions. A nitrogen gas laser (337 nm, with pulse width of 600 ps), which can be absorbed by CI[39] and TP[58] units, induced photocurrent decay curves of the positive and negative charge carriers shown in Figure 9 (200°C, double logarithmic plot), for various external electric field strengths. Because the transient times are short, the charge carriers are of the electronic type (i.e., holes and electrons); ionic carriers can safely be excluded as they drift much slower in the highly viscous discotic LC mesophases.[3] It is obvious that both the positive and negative charge carrier current decay curves are non-dispersive and that the drift times
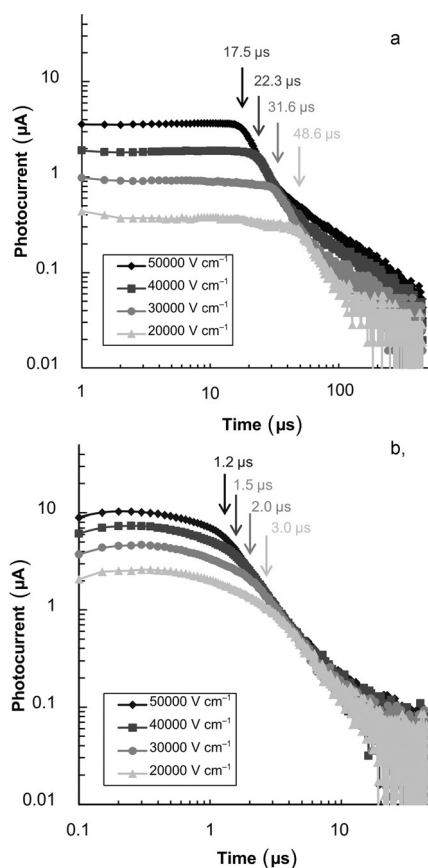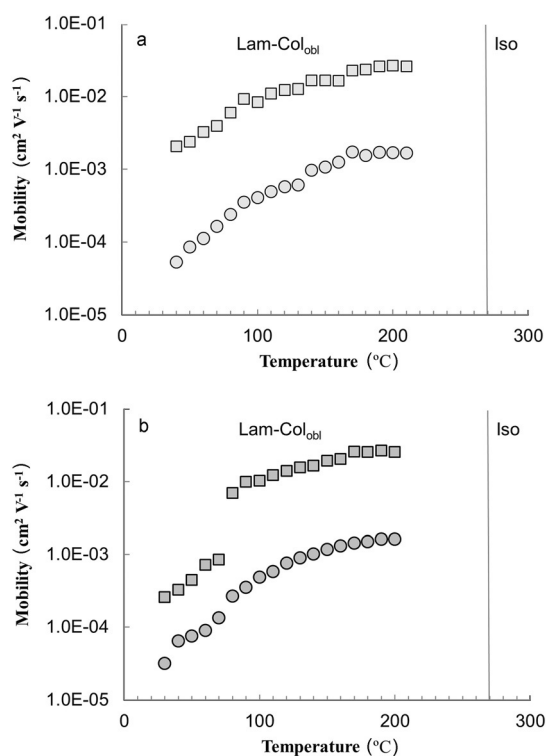
Figure 9. Double logarithmic plots of photo-induced hole (a) and electron (b) transient photocurrent curves for CI-TP2 under different external electric field strength (V cm^{-1}). $T=200\,^{\circ}$C (cooling process), and cell thickness = 15.6 μm. The flight times are directly labelled on the curves.

Figure 10. Temperature-dependency plots of charge carrier mobility for triad CI-TP2. a) Mobility measured during the cooling process from 210 to 40 °C; no sharp decrease below 80 °C for electron transport (■, μ_e; ●, μ_h); b) Mobility measured during the heating run from 30 to 200 °C, for which the sample cell was filled in as isotropic liquid of the sample by capillary phenomenon and slowly cooled to room temperature and kept for several days (■, μ_e; ●, μ_h). It is likely that some defects or grain boundaries have formed during this process, and became self-healed when the temperature was raised above 70 °C, explaining the mobility jump on heating (see the main text). The electron mobility turns out to be more sensitive to this phenomenon.

can be read accurately. This makes the TOF mobilities unambiguous. The holes transport curves of CI-TP2 at 200 °C under various electric field strengths are shown in Figure 9 (top): the measured photocurrent transit time of holes through the cell with thickness 15.6 μm is 17.5 μs under electric field of 5.0×10^4 V cm^{-1}, and the rate of the hole mobility is 1.8×10^{-3} cm^2 V^{-1} s^{-1}. The charge mobility was calculated by the equation: $\mu=d\,t_T^{-1}E^{-1}$, in which d is the sample thickness, t_T, the transit time, and E, the external electric field strength applied.

The transient photocurrent decay curves for electron transport of CI-TP2 at 200 °C are displayed in Figure 9 (bottom). The curves display shorter drift times of electrons through the cell than that of holes: the transit time is 1.2 μs under corresponding electric field of 5.0×10^4 V cm^{-1}, whereas the mobility $\mu_e = 2.6\times10^{-2}$ cm^2 V^{-1} s^{-1} at 200 °C, exhibits the characteristic of electric field independence.

The charge mobilities of the hole and electron are however dependent on the temperature. The mobility rates of CI-TP2 at various temperatures are shown in Figure 10 (top, for the cooling run; bottom for the heating run). From 30 to 210 °C, both μ_e and μ_h gradually increase: μ_e, from 10^{-4} to 10^{-2} cm^2 V^{-1} s^{-1}, and μ_h, from 10^{-5} to 10^{-3} cm^2 V^{-1} s^{-1}. The mobility of electrons is therefore much higher than that of holes at 200 °C: $\mu_e = 2.6\times10^{-2}$ cm^2 V^{-1} s^{-1}; $\mu_h = 1.8\times10^{-3}$ cm^2 V^{-1} s^{-1}. To our best knowl-

edge, this is the first example of mesophase semiconductor possessing such a large electronic μ_e/μ_h ratio (about 15).[3]

Comparing charge mobilities on both cooling and heating between 30 to 210 °C also reveals interesting features. In the high temperature range, the heat and cool curves are quasi-superimposable, and mobilities gradually decrease with temperature. Nevertheless, the mobilities are initially lower on heating below 70 °C, and undergo an abrupt increase from 70 to 80 °C. This change, not detected by DSC likely due to a difference of confinement, might originate from the healing of defects at domain boundaries, which would have formed during the crystallization process, while maintaining the sample in the ITO cell at room temperature for several days. As this phenomenon did not reproduce on cooling, mobilities close to room temperature remain about ten times higher than the initial ones.

The remarkable increase of charge carrier mobility of CI-TP2 with temperature is obviously related to the enhancement of the conformational mobility of the $-(CH_2)_3-$ spacer between the central CI core and the TP moieties. At higher temperatures the conjugated moieties attached to the spacer are free to move, to the effect that the overlapping within the segregated coronenediimide and triphenylene columns is improved, and thus the charge carrier mobility increased.[71,72]

The high ratio of electron and hole mobility results from the choice of the coupling of the conjugated species. In fact, it is known that the charge mobility increases with the extension of the π-conjugated system,[73] and coronenediimide is larger than triphenylene. Coronenediimide has been recognized as a n-type semiconductor with electron-transport capability,[39, 40] whereas triphenylene discotic columns are mainly hole transporters.[19, 20] Therefore, the self-organization of the CI-TP2 D–A–D triad enables the holes to hop along the one-dimensional π–π stacked triphenylene columns, and electrons to drift faster along the two-dimensional highly ordered packed coronenediimide lamellae, realizing a molecular heterojunction with segregated hole and electron-transport freeways.

Conclusion

A new family of donor–acceptor discotic-based triads, forming mesomorphic semiconductors with long-range ordered supramolecular architectures and high electronic charge mobility, namely PI-TP2, BI-TP2, CI-TP2 and its regioisomer, have been designed and synthesized for their potential uses in optoelectronic devices. The standard Pd and Pd/Cu-catalyzed Sonogashira coupling reactions have been applied to covalently link two TP discogens with PI chromophore for the construction of PI-TP2, which is further transformed to BP-TP2 by partial cyclization in pyridine, or totally transformed to CI-TP2 by DBU-promoting the annulation reaction. As the triads possess different π-conjugated systems, they display different colors and UV/Vis absorption spectra in solution, whose maxima are blueshifted with the conjugation modification. The photo-excited charge transfer between TP and PI units, resulting in completely fluorescence quenching of PI-TP2, and the other triads, showing efficient energy transfer between the donor and acceptor, implied that these triad systems are good D–A molecular heterojunction with TP as donor and arylene diimide as acceptor. POM, DSC, and SAXS showed that the triads self-organize into lamello-columnar oblique (LamCol$_{obl}$) mesophases over a wide temperature range including room temperature. The segregation between the electron-donor and the electron-acceptor moieties into separate rows and columnar stacks, respectively, has been promoted by linking through short lipophilic spacers, two types of aromatic core structures with different shape, size, and opposite electronic properties. These two regions are perfectly isolated from each other by the insulating molten aliphatic chains continuum, which bode well for enhanced conductivity properties. The high-resolution STM technique revealed the ordered assembly of PI-TP2 on the HOPG surface, and the segregation between the TP and diimine derivatives, in good agreement with the packing model deduced in the bulk mesophase. Most importantly, we demonstrated that for CI-TP2, the π–π stacked triphenylene columns act solely as hole hopping channels, leading to TOF hole mobility of 1.8×10^{-3} cm^{2}V^{-1}s^{-1} at 200 °C, whereas the rows of coronenediimide-cores play the role of electron-transport pathways and result in electron mobility of 2.6×10^{-2} cm^{2}V^{-1}s^{-1}. To our best knowledge, this is the first example of DLC oligomer showing an electron mobility about 15 times larger than the hole mobi-

lity, evidently due to the co-existence of two different interlocked and immiscible transportation pathways. The rational molecular engineering for D–A–D discotic triads, the highly segregated LamCol$_{obl}$ mesophase structure, and the unambiguous fast electron and hole mobilities imply strongly that these triads are suitable for organic photovoltaic cells applications. It should be stressed here that even higher charge carrier mobility would be obtained with these materials once homeotropic alignment could be realized in the ITO cells, what would remain a technical challenge to solve. The designed D–A–D triads architecture realized our initial goal to elaborate mesomorphous materials with positional long-range ordering and segregated A and D domains, validating a promising route to optimize materials with two distinct and conductive channels by self-sorting.

[1] S. Chandrasekhar, B. K. Sadashiva, K. A. Suresh, *Pramana* **1977**, *9*, 471–480.

[2] S. Kumar, *Chemistry of Discotic Liquid Crystals: From Monomers to Polymers*, CRC, Taylor and Francis Group, LLC, **2011**.

[3] R. J. Bushby, S. M. Kelly, M. O'Neill, *Springer Series in Material Sciences, Vol. 169: Liquid Crystalline Semiconductors: Materials, Properties and Applications*, Springer, Berlin, Heidelberg, **2013**.

[4] R. J. Bushby, K. Kawata, *Liq. Cryst.* **2011**, *38*, 1415–1426.

[5] S. Laschat, A. Baro, N. Steinke, F. Giesselmann, C. Hagele, G. Scalia, R. Judele, E. Kapatsina, S. Sauer, A. Schreivogel, M. Tosoni, *Angew. Chem. Int. Ed.* **2007**, *46*, 4832–4887; *Angew. Chem.* **2007**, *119*, 4916–4973.

[6] S. Sergeyev, W. Pisula, Y. H. Geerts, *Chem. Soc. Rev.* **2007**, *36*, 1902–1929.

[7] Y. Shimizu, K. Oikawa, K. Nakayama, D. Guillon, *J. Mater. Chem.* **2007**, *17*, 4223–4229.

[8] B. R. Kaafarani, *Chem. Mater.* **2011**, *23*, 378–396.

[9] T. Kato, T. Yasuda, Y. Kamikawa, M. Yoshio, *Chem. Commun.* **2009**, 729–739.

[10] S. K. Pal, S. Setia, B. S. Avinash, S. Kumar, *Liq. Cryst.* **2013**, *40*, 1769–1816.

[11] M. O'Neill, S. M. Kelly, *Adv. Mater.* **2011**, *23*, 566–584.

[12] W. Pisula, X. Feng, K. Müllen, *Adv. Mater.* **2010**, *22*, 3634–3649.

[13] W. Pisula, M. Zorn, J. Y. Chang, K. Müllen, R. Zentel, *Macromol. Rapid Commun.* **2009**, *30*, 1179–1202.

[14] E. K. Fleischmann, R. Zentel, *Angew. Chem. Int. Ed.* **2013**, *52*, 8810–8827; *Angew. Chem.* **2013**, *125*, 8972–8991.

[15] X. Feng, V. Marcon, W. Pisula, M. R. Hansen, J. Kirkpatrick, F. Grozema, D. Andrienko, K. Kremer, K. Müllen, *Nat. Mater.* **2009**, *8*, 421–426.

[16] K. Q. Zhao, C. Chen, H. Monobe, P. Hu, B. Q. Wang, Y. Shimizu, *Chem. Commun.* **2011**, *47*, 6290–6292.

[17] A. Demenev, S. H. Eichhorn, T. Taerum, D. F. Perepichka, S. Patwardhan, F. C. Grozema, L. D. A. Siebbeles, R. Klenkler, *Chem. Mater.* **2010**, *22*, 1420–1428.

[18] V. Percec, M. Glodde, T. K. Bera, Y. Miura, I. Shiyanovskaya, K. D. Singer, V. S. K. Balagurusamy, P. A. Heiney, I. Schnell, A. Rapp, H. W. Spiess, S. D. Hudson, H. Duan, *Nature* **2002**, *417*, 384 – 387.

[19] D. Adam, F. Closs, T. Frey, D. Funhoff, D. Haarer, H. Ringsdorf, P. Schumacher, K. Siemensmeyer, *Phys. Rev. Lett.* **1993**, *70*, 457 – 460.

[20] D. Adam, P. Schuhmacher, J. Simmerer, L. Haüssling, K. Siemensmeyer, K. H. Etzbachi, H. Ringsdorf, D. Haarer, *Nature* **1994**, *371*, 141 – 143.

[21] Y. Hirai, H. Monobe, N. Mizoshita, M. Moriyama, K. Hanabusa, Y. Shimizu, T. Kato, *Adv. Funct. Mater.* **2008**, *18*, 1668 – 1675.

[22] N. Mizoshita, H. Monobe, M. Inoue, M. Ukon, T. Watanabe, Y. Shimizu, K. Hanabusa, T. Kato, *Chem. Commun.* **2002**, 428 – 429.

[23] F. Würthner, *Chem. Commun.* **2004**, 1564 – 1579.

[24] C. Huang, S. Barlow, S. R. Marder, *J. Org. Chem.* **2011**, *76*, 2386 – 2407.

[25] X. Zhan, A. Facchetti, S. Barlow, T. J. Marks, M. A. Ratner, M. R. Wasielewski, S. R. Marder, *Adv. Mater.* **2011**, *23*, 268 – 284.

[26] C. Li, H. Wonneberger, *Adv. Mater.* **2012**, *24*, 613 – 636.

[27] E. Kozma, M. Catallani, *Dyes Pigm.* **2013**, *98*, 160 – 179.

[28] F. Würthner, C. Thalacker, S. Diele, C. Tschierske, *Chem. Eur. J.* **2001**, *7*, 2245 – 2253.

[29] Z. Chen, U. Baumeister, C. Tschierske, F. Würthner, *Chem. Eur. J.* **2007**, *13*, 450 – 465.

[30] A. Wicklein, A. Lang, M. Muth, M. Thelakkat, *J. Am. Chem. Soc.* **2009**, *131*, 14442 – 14453.

[31] Z. An, J. Yu, S. C. Jones, S. Barlow, S. Yoo, B. Domercq, P. Prins, L. D. A. Siebbeles, B. Kippelen, S. R. Marder, *Adv. Mater.* **2005**, *17*, 2580 – 2583.

[32] C. W. Struijk, A. B. Sieval, J. E. J. Dakhorst, M. van Dijk, P. Kimkes, R. B. M. Koehorst, H. Donker, T. J. Schaafsma, S. J. Picken, A. M. van deCraats, J. M. Warman, H. Zuilhof, E. J. R. Sudhölter, *J. Am. Chem. Soc.* **2000**, *122*, 11057 – 11066.

[33] L. Schmidt-Mende, A. Fechtenkotter, K. Müllen, E. Moons, R. H. Friend, J. D. MacKenzie, *Science* **2001**, *293*, 1119 – 1122.

[34] Y. Zhang, H. Wang, Y. Xiao, L. Wang, D. Shi, C. Cheng, *ACS Appl. Mater. Interfaces* **2013**, *5*, 11093 – 11100.

[35] M.-A. Muth, G. Gupta, A. Wicklein, M. Carrasco-Orozco, T. Thurn-Albrecht, M. Thelakkat, *J. Phys. Chem. C* **2014**, *118*, 92 – 102.

[36] M. Funahashi, A. Sonoda, *Org. Electron.* **2012**, *13*, 1633 – 1640.

[37] V. Dehm, Z. Chen, U. Baumeister, P. Prins, L. D. A. Siebbeles, F. Würthner, *Org. Lett.* **2007**, *9*, 1085 – 1088.

[38] U. Rohr, P. Schlichting, A. Böhm, M. Gross, K. Meerholz, C. Bräuchle, K. Müllen, *Angew. Chem. Int. Ed.* **1998**, *37*, 1434 – 1437; *Angew. Chem.* **1998**, *110*, 1463 – 1467.

[39] U. Rohr, C. Kohl, K. Müllen, A. van de Craats, J. Warman, *J. Mater. Chem.* **2001**, *11*, 1789 – 1799.

[40] Z. An, J. Yu, B. Domercq, S. C. Jones, S. Barlow, B. Kippelen, S. R. Marder, *J. Mater. Chem.* **2009**, *19*, 6688 – 6698.

[41] T. Yang, J. Pu, J. Zhang, W. Wang, *J. Org. Chem.* **2013**, *78*, 4857 – 4866.

[42] J. Eccher, G. C. Faria, H. Bock, H. von Seggern, I. H. Bechtold, *ACS Appl. Mater. Interfaces* **2013**, *5*, 11935 – 11943.

[43] L. Dong, W. Li, W.-S. Li, *Nanoscale* **2011**, *3*, 3447 – 3461.

[44] M. Wang, F. Wudl, *J. Mater. Chem.* **2012**, *22*, 24297 – 24314.

[45] J. Wu, J. Qu, N. Tchebotareva, K. Müllen, *Tetrahedron Lett.* **2005**, *46*, 1565 – 1568.

[46] E. Peeters, P. A. van Hal, S. C. J. Meskers, R. A. J. Janssen, E. W. Meijer, *Chem. Eur. J.* **2002**, *8*, 4470 – 4474.

[47] M. Bagui, T. Dutta, S. Chakraborty, J. S. Melinger, H. Zhong, A. Keightley, Z. Peng, *J. Phys. Chem. A* **2011**, *115*, 1579 – 1592.

[48] J. E. Bullock, R. Carmielie, S. M. Mickley, J. Vura-Weis, M. R. Wasielewski, *J. Am. Chem. Soc.* **2009**, *131*, 11919 – 11929.

[49] L. F. Dössel, V. Kamm, I. A. Howard, F. Laquai, W. Pisula, X. Feng, C. Li, M. Takase, T. Kudernac, S. de Feyter, K. Müllen, *J. Am. Chem. Soc.* **2012**, *134*, 5876 – 5886.

[50] J. M. Mativetsky, M. Kastler, R. C. Savage, D. Gentilini, M. Palma, W. Pisula, K. Müllen, P. Samori, *Adv. Funct. Mater.* **2009**, *19*, 2486 – 2494.

[51] H. Hayashi, W. Nihashi, T. Umeyama, Y. Matano, S. Seki, Y. Shimizu, H. Imahori, *J. Am. Chem. Soc.* **2011**, *133*, 10736 – 10739.

[52] W. S. Li, Y. Yamamoto, T. Fukushima, A. Saeki, S. Seki, S. Tagawa, H. Masunaga, S. Sasaki, M. Takata, T. Aida, *J. Am. Chem. Soc.* **2008**, *130*, 8886 – 8887.

[53] W. S. Li, A. Saeki, Y. Yamamoto, T. Fukushima, S. Seki, N. Ishii, K. Kato, M. Takata, T. Aida, *Chem. Asian J.* **2010**, *5*, 1566 – 1572.

[54] D. Zeng, I. Tahar-Djebbar, Y. Xiao, F. Kameche, N. Kayunkid, M. Brinkmann, D. Guillon, B. Heinrich, B. Donnio, D. A. Ivanov, E. Lacaze, D. Kreher, F. Mathevet, A.-J. Attias, *Macromolecules* **2014**, *47*, 1715 – 1731.

[55] L. Bu, X. Guo, B. Yu, Y. Qu, Z. Xie, D. Yan, Y. Geng, F. Wang, *J. Am. Chem. Soc.* **2009**, *131*, 13242 – 13243.

[56] R. Charvet, Y. Yamamoto, T. Sasaki, J. Kim, K. Kato, M. Takata, A. Saeki, S. Seki, T. Aida, *J. Am. Chem. Soc.* **2012**, *134*, 2524 – 2527.

[57] Y. Hizume, K. Tashiro, R. Charvet, Y. Yamamoto, A. Saeki, S. Seki, T. Aida, *J. Am. Chem. Soc.* **2010**, *132*, 6628 – 6629.

[58] X. Kong, Z. He, Y. Zhang, L. Mu, C. Liang, B. Chen, X. Jing, A. N. Cammidge, *Org. Lett.* **2011**, *13*, 764 – 767.

[59] S. K. Gupta, S. Setia, S. Sidiq, M. Gupta, S. Kumar, S. K. Pal, *RSC Adv.* **2013**, *3*, 12060 – 12065.

[60] V. Lemaur, D. A. da Silva Filho, V. Coropceanu, M. Lehmann, Y. Geerts, J. Piris, M. G. Debije, A. M. van de Craats, K. Senthilkumar, L. D. A. Siebbeles, J. M. Warman, J.-L. Bredas, J. Cornil, *J. Am. Chem. Soc.* **2004**, *126*, 3271 – 3279.

[61] K. Q. Zhao, G. F. Yang, W. H. Yu, B. Q. Wang, P. Hu, *Chin. J. Org. Chem.* **2009**, *29*, 2017 – 2020.

[62] B. Han, P. Hu, B. Wang, C. Redshaw, K.-Q. Zhao, *Beilstein J. Org. Chem.* **2013**, *9*, 2852 – 2861.

[63] F. Würthner, V. Stepanenko, Z. Chen, C. R. Saha-Möller, N. Kocher, D. Stalke, *J. Org. Chem.* **2004**, *69*, 7933 – 7939.

[64] S. Fabig, G. Haberhauer, R. Gleiter, *J. Am. Chem. Soc.* **2015**, *137*, 1833 – 1843.

[65] Y. Yang, C. Wang, *Chem. Soc. Rev.* **2009**, *38*, 2576 – 2589.

[66] K. S. Mali, J. Adisoejoso, E. Ghijsens, I. de Cat, S. de Feyter, *Acc. Chem. Res.* **2012**, *45*, 1309 – 1320.

[67] Y. Kaneda, M. E. Stawasz, D. L. Sampson, B. A. Parkinson, *Langmuir* **2001**, *17*, 6185 – 6195.

[68] R. Zhang, Q. F. Yan, Y. T. Shen, L. H. Gan, Q. D. Zeng, D. H. Zhao, C. Wang, *CrystEngComm* **2011**, *13*, 5566 – 5570.

[69] J. Lu, S. B. Lei, Q. D. Zeng, S. Z. Kang, C. Wang, L. J. Wan, C. L. Bai, *J. Phys. Chem. B* **2004**, *108*, 5161 – 5165.

[70] X. M. Zhang, H. F. Wang, S. Wang, Y. T. Shen, Y. L. Yang, K. Deng, K. Q. Zhao, Q. D. Zeng, C. Wang, *J. Phys. Chem. C* **2013**, *117*, 307 – 312.

[71] A. M. Van de Craats, L. D. A. Siebbeles, I. Bleyl, D. Haarer, Y. A. Berlin, A. A. Zharikov, J. M. Warman, *J. Phys. Chem. B* **1998**, *102*, 9625 – 9634.

[72] I. Paraschiv, M. Giesbers, B. van Lagen, F. C. Grozema, R. D. Abellon, L. D. A. Siebbeles, A. T. M. Marcelis, H. Zuilhof, E. J. R. Sudholter, *Chem. Mater.* **2006**, *18*, 968 – 974.

[73] A. M. Van de Craats, J. M. Warman, *Adv. Mater.* **2001**, *13*, 130 – 133.